Confined vs. eruptive M-class flares in solar cycles 23 and 24

Rositsa Miteva[1] and Werner Pötzi[2]
[1] Institute of Astronomy and National Astronomical Observatory - Bulgarian Academy of Sciences, 1784 Sofia, Bulgaria
[2] Institute of Physics, Kanzelhöhe Observatory for Solar and Environmental Research, University of Graz, 8010 Graz, Austria
rmiteva@nao-rozhen.org
(Submitted on 09.04.2025; Accepted on 25.04.2025)

Abstract. This report presents a quantitative comparison between confined, eruptive and all (2177) M-class solar flares (SFs) over the last two solar cycles (SC) and separately in SC 23 and 24. The properties of the SFs, related radio bursts and the parent sunspots (Hale type and total area) are examined. The differences are presented and discussed in the framework of space weather.
Key words: solar flares; solar cycle; sunspot type

1 Introduction

The most energetic explosions in the solar corona are the solar flares (SFs), reaching up to 10^{25} Joules [Shibata and Magara, 2011]. The name portrays the flash seen on solar images in different wavelengths. However, a SF represents a collection of phenomena, from the overall restructuring of magnetic fields in the active region (AR), to particle acceleration, mass motion, and electromagnetic (EM) emission over a range of wavelengths and intensities. Due to the long-standing data[3] available from the Geostationary Operational Environmental Satellite (GOES) sequence of satellites since the mid-1970s, the SF strength (or more commonly known as a class) is defined according to the soft X-ray (SXR) flux in the 1–8 Å channel[4]. The strongest SFs are termed X ($\geq 10^{-4}$ W m^2), followed by M, C, B, and A, where each class is 10 times less intense[5].

Apart from plasma jets, during the flaring process large volumes of coronal plasma with embedded magnetic fields are expelled towards the interplanetary (IP) space. Usually observed in white light, these plasma blobs are called coronal mass ejections (CMEs), [Webb and Howard, 2012]. Moreover, their presence is an important evidence for the eruptive character of solar activity.

Associated with the SFs and CMEs are the particles from the corona that gyrate along the field lines. When those field lines are open (namely, starting from the solar photosphere and closing at infinity), the energetic protons, electrons, and heavy ions can be detected by in situ instruments connected to the same magnetic field lines. The collective term used for this phenomenon is solar energetic particles (SEPs) [Desai and Giacalone, 2016].

Alternatively, if the local plasma conditions are suitable and the particle population has the necessary properties, the energetic electrons can lead to an emission of radio waves [Melrose, 1980]. Depending on the trajectory of the driver (or the local accelerator), these radio waves leave a distinctive mark

[3] ftp://ftp.ngdc.noaa.gov/STP/space-weather/solar-data/solar-features/
[4] https://www.swpc.noaa.gov/products/goes-x-ray-flux
[5] https://solarmonitor.org/

when visualized in a so-called dynamic radio spectrum (i.e., frequency vs. time-plot, where the radio intensity is color-coded). The different tracks are termed radio bursts and are historically grouped into five main radio burst types [Wild et al., 1963] due to their most probable cause, namely, I: noise storm; II: shock waves; III: electron beams; IV: trapped electrons; V: post-type III continuum. The different types also have different space weather potential [Warmuth and Mann, 2004]. For example, the association between SFs and selective radio bursts was explored in details by [Miteva, 2021, Miteva and Samwel, 2022].

All solar activity agents described above (i.e., SFs, CMEs, SEPs and radio bursts) have effects on the planetary magnetospheres and atmospheres (e.g., in terms of large-scale disturbances known as geomagnetic storms [Gonzalez et al., 1994]), on the technological devices in space and on ground (e.g., failures, deterioration, malfunction [Miteva et al., 2023]) and/or on human health (e.g., radiation exposures [Semkova et al., 2018]). The collection of such short-term effects (from minutes to about one solar rotation) is known as space weather [Pulkkinen, 2007, Temmer, 2021]. The successful forecast of the occurrence and strength of these space weather events is a key research topic that currently accumulates the theoretical and novel machine learning efforts.

The concept of eruptivity and confinement of SFs has already been explored previously, starting from, e.g. [Svestka, 1986]. The previous studies agree that eruptive SFs tend to occur in smaller ARs with weaker magnetic field strengths, their flare ribbons have weaker mean magnetic field strengths, and the reconnection process incorporates larger fractions of the AR, e.g., [Kazachenko, 2023]. Without the ambition to do a comprehensive review (see e.g. [Miteva, 2021] and the references therein), some main results from a selection of (large) statistical works are outlined below.

- A representative study on SC24 was reported by [Li et al., 2020], covering 322 GOES SFs larger than M1.0 (2010–2019). They found that confined SFs originate from ARs with an unsigned magnetic flux larger than 1.0×10^{23} Mx (in 93% of the cases).
- An expansion of the above list was completed by [Li et al., 2021], based on an analysis of 719 SFs larger than C5.0 (2010–2019). SFs with a larger total unsigned magnetic flux tend to be confined and the latter also tend to have larger values of the length of steep gradient polarity-inversion line, total photospheric free magnetic energy, and areas with large shear angle.
- New parameters were proposed by [Li et al., 2022] based on a study of 106 GOES SFs larger than M1.0 (2010–2019). Namely, in about 90% of all eruptive SFs, the ratio of the mean characteristic twist parameters within the flaring polarity inversion line region to the total unsigned magnetic flux and the ratio of the mean characteristic twist parameters within the area of high photospheric magnetic free energy density to the total unsigned magnetic flux are both beyond their respective critical values (2.2×10^{-24} and 3.2×10^{-24} Mm^{-1} Mx^{-1}), whereas they are less than these critical values in about 80% of confined SFs.
- Another comprehensive database was provided by [Kazachenko, 2023], based on SDO data, analyzing 480 SFs above C5.0 in the period 2010 to April 2016. The new result is that confined SFs have higher mean peak reconnection rates compared to eruptive SFs.

In contrast to the above, other previous studies focused exclusively on selected event samples. For example, a study by [Maity et al., 2024] on 26 eruptive and 11 confined SFs (2011–2017) indicated that the total change in the Lorentz force for confined SFs is below 1.8×10^{22} dyn. Another study focused on specific ARs and showed that the ratio of current-carrying to total helicity indicates a potential for eruptions [Thalmann et al., 2019].

A proxy for SF confinement is the lack of associated plasma eruptions. It was already shown [Miteva, 2021] that among all X-class SFs in SCs 23 and 24, 133/175 (76%) were found to be eruptive and 23/175 (13%) had no CME signatures. The analysis was then extended to M-class SFs.

That is, a sample of all M-class SFs in SCs 23 and 24 (2177 events) was reported by [Miteva and Samwel, 2022]. In contrast to predominantly eruptive X-class SFs, M-class SFs were shown to be accompanied by CMEs only in 41% (889/2177) of the cases that will be regarded as eruptive. Furthermore, a minority of the entire sample, 133 or 6% (247 or 11%), was accompanied by in situ protons (electrons) and 1078 or 50% (148 or 7%) by type III (II) radio bursts, respectively. A SF-associated CME/SEP/radio burst was identified where possible; however, the study did not explore any confinement issues, which will be considered here.

The purpose of this work is to fully explore the available database of M-class SFs from [Miteva and Samwel, 2022] (which will be noted as Paper I) together with their identified associations and accompanied activity phenomena during the last two SCs (1996–2019). The main advantage of this event list is the wider temporal coverage than previously reported, namely also including the entire SC23. This is advantageous for performing statistical studies and exploring differences between the SCs as well. In addition, we perform a comparison between the parameters of the confined and eruptive M-class SFs with a focus on their parent sunspot configurations and area. The results are discussed in the context of space weather.

2 Methodology

This study is based on the analyses of all M-class SFs performed on SCs 23 and 24 (Paper I) with a focus on confined SFs.

We adopted the well-accepted definition for a confined SF to be one without an associated plasma eruption (i.e., a CME) from the same AR. Based on the original sample of 2177 M-class SFs over SCs 23 and 24, those with no relevant CME amount to 989, which will be further considered as confined M-class SFs. We note that this value should be regarded as an upper limit for the confined sample. The reason for this is that the lack of a CME signature could be due to misidentification by the observer or other subjectivity, insufficient instrument sensitivity, and/or data coverage and thus the 'real' number of confined M-class SFs would be smaller. The usage of multi-instrument data sources and multi-observer identifications could potentially minimize such a bias. Nevertheless, for this study we will keep the sample of 989 so-identified SFs as the confined M-class SFs. Furthermore, the sum of the confined and eruptive SFs is less than that of all detected M-class SFs, as a handful of uncertain cases were discarded from the statistics.

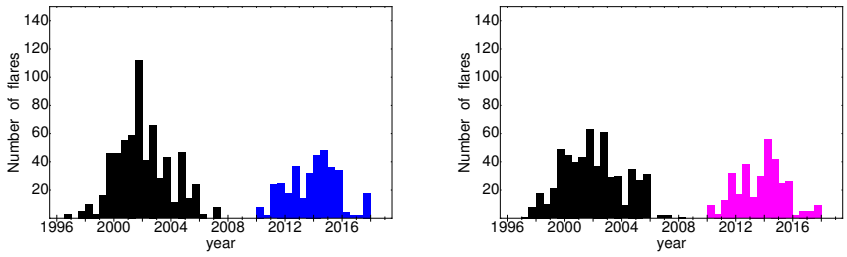

Fig. 1. Yearly distribution of the number of confined (left) and eruptive (right) M-class SFs. In black color are denoted the SFs in SC23, whereas in blue/magenta, the ones in SC24, respectively.

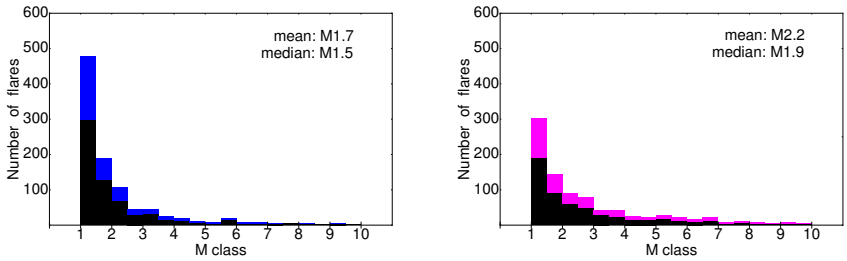

Fig. 2. Class distribution of the confined (left) and eruptive (right) M-class SFs. Color codes as in Fig. 1

3 Results

The results are structured as a comparison between the confined sub-samples (on the left side of the figures) and eruptive sub-samples (on the right). The plots (Figs. 1–6) depict the relevant distributions over the entire time period only (SCs 23 and 24) in order to avoid redundancies. However, the mean/median values of the respective M-class SFs are calculated separately for SC23, SC24, SCs 23 and 24 and are listed in Table 1.

3.1 M-class SF properties

The yearly histograms are shown in Fig. 1 for the confined and eruptive SFs. In black color will be shown the distributions in SC23, whereas the color depicts the respective numbers in SC24. The decrease in the number of M-class SFs in SC24 can be easily noticed, with 45% decline for the confined and 42% for the eruptive sub-samples (the decline of all M-class flares was reported to be 47%).

The distribution of the GOES SXR class is shown in Fig. 2, and the majority of the SFs are in fact of M1 and M2 classes. The mean and median values

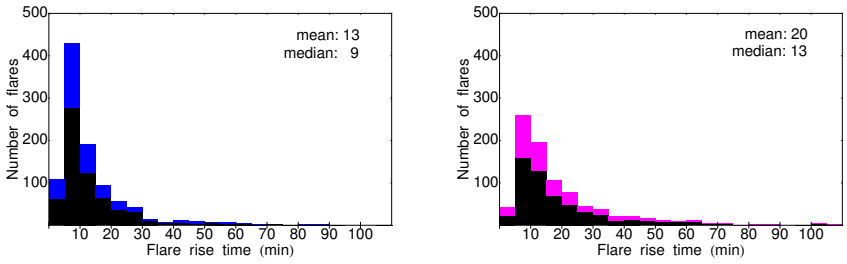

Fig. 3. Rise time for the confined (left) and eruptive (right) M-class SFs. Color code as in Fig. 1.

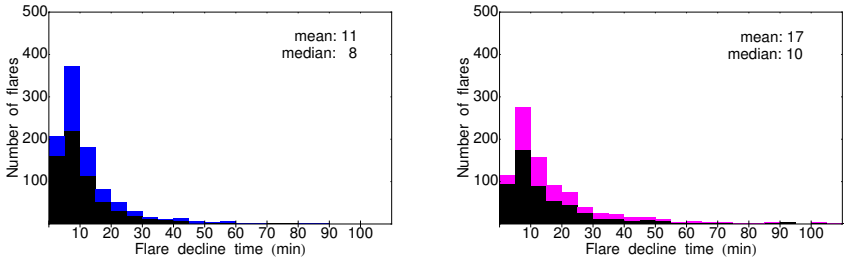

Fig. 4. Decline time for the confined (left) and eruptive (right) M-class SFs. Color code as in Fig. 1.

for both sub-samples are shown in each plot for the entire time period. The mean/median values in SCs 23 and 24 for eruptive M-class SF (M2.2/M1.9) are slightly higher compared to the confined sample (M1.7/M1.5), respectively. The trends obtained in each of the SCs (see Table 1) follow that of the entire sample.

Similarly to Paper I, we present the histograms of the rise (peak-to-maximum) and decline (maximum-to-end) SF times, see Figs. 3 and 4. Overall, the eruptive M-class SFs show longer periods for the rise and decline times compared to the confined (and the entire) M-class SF sample. This tendency is also kept for each individual SC; see Table 1.

Finally, we show the histograms for the SF longitude in Figs. 5. Despite the bulge at the disk center-to-Western longitudes for the confined SFs, the distribution for the eruptive SFs shows slight peaks around/beyond the mid-longitudes. For the SF latitude, Fig. 6, a quantitative assessment is provided in terms of mean/median values, with the tendency towards Southern latitudes for both sub-samples. Confined SFs are exclusively Southern phenomena as a sample, however the eruptive SFs shift to center-to-Northern latitudes in SC23 (Table 1).

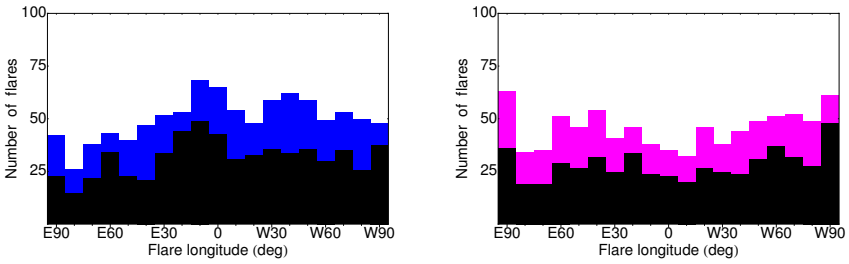

Fig. 5. Longitude for the associated ARs of confined (left) and eruptive (right) M-class SFs. Color code as in Fig. 1.

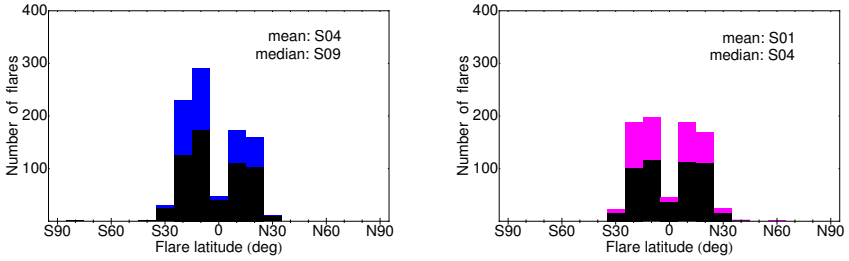

Fig. 6. Latitude for the associated ARs of confined (left) and eruptive (right) M-class SFs. Color code as in Fig. 1.

Using hemispheric sunspot numbers[6], for SC24 the South excess can be estimated to occur between 2013.5 and 2015.5. In combination with the fact that the majority of SFs were detected in this time period (see Fig. 1), one would expect the mean latitude to be (well in the) south. However, since the SC was already not so young at this time, the high latitudes of the early SFs move the mean value to the North (SC24 was in the beginning North dominated). This was not sufficient to cancel the southern trend for SC24, but instead led to a reduction in the mean/median values.

In addition, we inspected the sunspot areas for the different types of SFs. The data was taken from the Solar Region Summaries of the Space Weather Prediction Center[7]. The results are summarized in Table 1 and demonstrate that confined SFs originate from considerably larger sunspot areas (over 600 μhem in mean values), compared to the eruptive SFs (about 420 μhem in mean values). The median values are also calculated and, in general, are much smaller (up to one-third) than the mean (average) ones. This trend (in mean or median values) is kept during all considered time periods.

[6] https://sidc.be/SILSO/home
[7] `https://www.swpc.noaa.gov/products/solar-region-summary`

Table 1. Mean/median values for the different M-class samples and parameters, respectively. For completeness, we add the values for the entire sample of M-class flares (denoted with 'All') from [Miteva and Samwel, 2022]. The number of SFs in each time period are given in a bold font.

Parameter	Confined	Eruptive	All
SCs 23+24	**989**	**889**	**2177**
class	M1.7/M1.5	M2.2/M1.9	M2.0/M1.7
rise time (min)	13/9	20/13	16/10
decline time (min)	11/8	17/10	13/8
sunspot area (μhem)	608/420	420/260	523/340
latitude (degrees)	S04/S09	S01/S04	S02/S07
SC23	**640**	**562**	**1428**
class	M1.8/M1.5	M2.2/M1.9	M2.0/M1.7
rise time (min)	14/9	20/13	16/11
decline time (min)	11/8	17/10	14/9
sunspot area (μhem)	610/423	426/250	527/330
latitude (degrees)	S03/S08	N01/N02	S01/S05
SC24	**349**	**327**	**749**
class	M1.7/M1.4	M2.2/M2.0	M1.9/M1.6
rise time (min)	12/8	20/13	16/10
decline time (min)	13/8	20/13	16/10
sunspot area (μhem)	604/370	411/270	515/330
latitude (degrees)	S05/S12	S02/S09	S04/S10

3.2 Sunspot magnetic configurations

The adopted Hale type of sunspot magnetic configuration [Hale et al., 1919] is as described in `https://www.spaceweather.com/glossary/magneticclasses.html`.

The results on the sunspot Hale type (reported on the same day as the SF occurrence) are summarized in Table 2. The sunspots and the confined/eruptive SFs are paired based on the same AR or/and location. We reported the numbers of the different Hale types for the confined and eruptive SFs separately in SC23, SC24 and both SCs and calculated the percentages as a ratio to the event sample. The sample sizes for each case are given in bold fonts in Table 2. For completeness, the same is done for the entire sample of M-class SFs.

The sum of the reported numbers in SC23 and SC24 gives the value for SCs 23 and 24. However, this is not the case for the percentages (shown in parentheses), since they are calculated to a different sample size. For comparison purposes, we use the normalized values (that is, the percentages) to minimize any bias due to the event imbalance observed in SCs 23 and 24.

Overall, when comparing the confined and eruptive SF samples, the similar percentages are obtained for a given sunspot Hale type, within the uncertainties, with the exception of β-γ-δ type: The cases in the confined subcategory (36%) are larger compared to the eruptive one (25%) over SCs 23 and 24 (with a difference of 11%). The same trends are found when we inspect the percentages separately for SC23 (8% more confined SFs) and in SC24 (17±1% more confined SFs). No δ-type configuration occurs in the entire sample of M-class SFs, and a very few cases of γ and γ-δ were found.

Table 2. Number of sunspots according to their Hale type (reported±uncertain), identified as the origin of confined vs. eruptive M-class SFs. For completeness, we add the values for the entire sample of M-class flares (denoted with 'All') from [Miteva and Samwel, 2022]. In parenthesis the values (in percentage) normalized to the respective sample size, after rounding are given.

Hale type	**Confined**	**Eruptive**	**All**
SCs 23+24	**989**	**889**	**2177**
α	29 ± 20 (3 ± 2%)	37 ± 25 (4 ± 3 %)	76 ± 50 (3 ± 2%)
β	226 ± 39 (23 ± 4%)	253 ± 56 (28 ± 6%)	546 ± 109 (25 ± 5%)
γ	6	–	6
β-γ	210 ± 11 (21 ± 1%)	177 ± 10 (20 ± 1%)	459 ± 22 (21 ± 1%)
β-δ	23 (2%)	24 (3%)	48 (2%)
β-γ-δ	353 ± 2 (36%)	224 (25%)	661 ± 2 (30%)
γ-δ	3	–	4
no sunspots	–	31 (3%)	51 (2%)
uncertain	27 (3%)	50 (6%)	135 (6%)
SC23	**640**	**562**	**1428**
α	26 ± 10 (4 ± 2%)	20 ± 17 (4 ± 3%)	55 ± 31 (4 ± 2%)
β	164 ± 24 (26 ± 4%)	183 ± 38 (33 ± 7%)	397 ± 70 (28 ± 5%)
γ	6	–	6
β-γ	135 ± 5 (21 ± 1%)	100 ± 4 (18 ± 1%)	289 ± 9 (20 ± 1%)
β-δ	16 (2%)	11 (2%)	28 (2%)
β-γ-δ	196 (31%)	131 (23%)	385 (27%)
γ-δ	3	–	4
no sunspots	–	14 (2%)	22 (2%)
uncertain	27 (4%)	42 (7%)	124 (9%)
SC24	**349**	**327**	**749**
α	3 ± 10 (1 ± 3%)	17 ± 8 (5 ± 2%)	21 ± 19 (3 ± 3%)
β	62 ± 15 (18 ± 4%)	70 ± 18 (21 ± 6%)	149 ± 39 (20 ± 12%)
γ	–	–	–
β-γ	75 ± 6 (21 ± 2%)	77 ± 6 (24 ± 1%)	170 ± 13 (23 ± 2%)
β-δ	7 (2%)	13 (4%)	20 (3%)
β-γ-δ	157 ± 2 (45 ± 1%)	93 (28%)	276 ± 2 (37%)
γ-δ	–	–	–
no sunspots	–	17 (5%)	29 (4%)
uncertain	–	8 (2%)	11 (1%)

3.3 Related radio bursts

The confined M-class SFs are accompanied by 317 type III radio bursts (or 32% of the entire confined sample, 989) distributed as: 190 clear signatures (19%), 40 denoted as weak, 66 as oculted, and 21 as weak and oculted. Among all these 317 cases, 226 (23%) type IIIs occur in the rise phase of the confined M-class SF, whereas 91 cases (9%) occur during the decline phase.

For completeness, we analyze the associated type II radio bursts, however we obtain only 14 confined M-class flares (about 1%) to be accompanied with type IIs. As the type II signatures are interpreted as shock motion in the corona, these 14 cases could be erroneously identified confinement cases or be used as a proxy for flare-related shock waves. The list is given below in chronological order with their date, class, onset time, location (or AR number) and sunspot Hale type:

– 1996–06–29, M1.6, 19:07, S14E01, β

– 2000–05–15, M1.1, 16:38, S15E51, β
– 2000–07–14, M3.7, 13:44, N20W08, β-γ-δ
– 2000–07–21, M1.7, 05:17, N12E10, β
– 2000–11–09, M1.0, 15:45, S11E10, β
– 2001–03-28, M4.3, 11:21, N18E02, β-γ-δ
– 2001–04–04, M1.6, 09:41, S21E68, β
– 2001–10–19, M1.2, 02:20, (AR 9661?), β-γ-δ
– 2002–07–26, M5.3, 22:03, (AR 10044?), β
– 2002–07–26, M4.6, 22:36, (AR 10044), β
– 2002–07–28, M2.2, 22:58, (AR 10044?), β-γ-δ
– 2002–08–14, M2.3, 01:47, N09W59, β
– 2003–03–19, M1.5, 02:58, S15W55, β-γ-δ
– 2003–11–05, M1.6, 02:37, S19W89, β-γ-δ

In either case, the exclusion of these cases from the confined category will not lead to statistically significant changes in the reported results.

4 Discussions

We completed the first statistical comparison of the properties of M-class SFs in SCs 23 and 24 (freely available at `https://catalogs.astro.bas.bg/`), their accompanied phenomena, and sunspot structures when separated into confined and eruptive subcategories according to the lack or presence of accompanied CME, respectively.

In contrast to the detailed magnetic flux and energy, twist, shear, current system, etc. measurements by the previous studies, in this work we focus on a large volume of events (over two SCs) with routinely measured and reported in catalogs SF properties, sunspot Hale type and area, as well as identified accompanied phenomena (e.g., Paper I).

Our results confirm that the confined M-class SFs are slightly weaker in GOES class and have slightly shorter (but not statistically significant) rise and decline times compared to the eruptive or/and to the entire population of M-class SFs in the given time periods. Also, the different samples of M-class flares tend to occur at Southern latitudes in all periods of interest, similarly to the X-class SFs [Miteva, 2021].

About 32% of the confined SFs show type III radio burst signatures, compared to 50% for the eruptive SFs (Paper I). This indicated that the ARs of confined SFs supports open field lines (more often during the SF rise time) that can guide the electrons giving rise to radio emission. However, the confined SF-magnetic configuration do not support a particle escape from the corona as there are virtually no SEPs found to be associated with confined SFs, which was also found for X-class flares by [Klein et al., 2011]. Thus, the detection of SEPs seems a more reliable proxy (in a statistical sense) for SF eruptivity (and thus for space weather forecasting) compared to the occurrence of type III bursts.

With respect to type IIs, the shock signatures associated with confined SFs seem to be a rare exception (about 1% of the cases), while 7% of eruptive SFs were associated with type IIs (paper I).

Our results confirm the well-known tendency for complex magnetic field configurations to impede eruptions. The confined M-class SFs in SCs 23 and 24 that originate at β-γ-δ are 11% more abundant compared to the eruptive sample. Also, a SC-dependence is noticed only for this sunspot configuration, as the latter sample is overrepresented by 17% in SC24 compared to SC23 (only 8%). Whether previous SCs show similar properties (namely producing more complex ARs) goes beyond the scope of this work. In summary, the Hale type of the sunspot alone, tends to have only a limited potential for space weather forecasting, even when combined with an increased AR potential during a particular SC.

In contrast to the Hale type, confined M-class SFs have a larger (by up to one third) sunspot area in mean or median values, compared to the eruptive ones. This is consistent with the behavior found by [Cliver et al., 2022, Kazachenko, 2023]. There, the authors found that the largest sunspot groups tend to produce confined SFs. We found that the tendency is independent on the SC. Thus, the sunspot area could be regarded as a promising parameter for SF eruptivity/confinement. However, proving a threshold value goes beyond the scope of the current study.

In summary, the knowledge that larger sunspot groups with more complex magnetic configurations have a higher probability of producing confined flares is also of interest for flare prediction and space weather forecast.

Acknowledgments

This research was funded by the Bulgarian National Science Foundation project No. KP-06-Austria/5 (14-08-2023) and Austria's Agency for Education and Internationalisation (OeAD) project No. BG 04/2023.

References

Cliver, E. W., Pötzi, W., and Veronig, A. M. (2022). Large Sunspot Groups and Great Magnetic Storms: Magnetic Suppression of CMEs. *ApJ*, 938(2):136.

Desai, M. and Giacalone, J. (2016). Large gradual solar energetic particle events. *Living Reviews in Solar Physics*, 13:3.

Gonzalez, W. D., Joselyn, J. A., Kamide, Y., Kroehl, H. W., Rostoker, G., Tsurutani, B. T., and Vasyliunas, V. M. (1994). What is a geomagnetic storm? *Journal of Geophysical Research*, 99(A4):5771–5792.

Hale, G. E., Ellerman, F., Nicholson, S. B., and Joy, A. H. (1919). The Magnetic Polarity of Sun-Spots. *ApJ*, 49:153.

Kazachenko, M. D. (2023). A Database of Magnetic and Thermodynamic Properties of Confined and Eruptive Solar Flares. *ApJ*, 958(2):104.

Klein, K. L., Trottet, G., Samwel, S., and Malandraki, O. (2011). Particle Acceleration and Propagation in Strong Flares without Major Solar Energetic Particle Events. *Sol. Phys.*, 269(2):309–333.

Li, T., Chen, A., Hou, Y., Veronig, A. M., Yang, S., and Zhang, J. (2021). Magnetic Flux and Magnetic Nonpotentiality of Active Regions in Eruptive and Confined Solar Flares. *ApJ*, 917(2):L29.

Li, T., Hou, Y., Yang, S., Zhang, J., Liu, L., and Veronig, A. M. (2020). Magnetic Flux of Active Regions Determining the Eruptive Character of Large Solar Flares. *ApJ*, 900(2):128.

Li, T., Sun, X., Hou, Y., Chen, A., Yang, S., and Zhang, J. (2022). A New Magnetic Parameter of Active Regions Distinguishing Large Eruptive and Confined Solar Flares. *ApJ*, 926(2):L14.

Maity, S. S., Sarkar, R., Chatterjee, P., and Srivastava, N. (2024). Changes in Photospheric Lorentz Force in Eruptive and Confined Solar Flares. *ApJ*, 962(1):86.

Melrose, D. B. (1980). The Emission Mechanisms for Solar Radio Bursts. *Space Sci. Rev.*, 26(1):3–38.

Miteva, R. (2021). Eruptive versus confined X-class flares in solar cycles 23 and 24. *Bulgarian Astronomical Journal*, 35:87.

Miteva, R. and Samwel, S. W. (2022). M-Class Solar Flares in Solar Cycles 23 and 24: Properties and Space Weather Relevance. *Universe*, 8(1):39.

Miteva, R., Samwel, S. W., and Tkatchova, S. (2023). Space Weather Effects on Satellites. *Astronomy*, 2(3):165–179.

Pulkkinen, T. (2007). Space Weather: Terrestrial Perspective. *Living Reviews in Solar Physics*, 4:1.

Semkova, J., Koleva, R., Benghin, V., Dachev, T., Matviichuk, Y., Tomov, B., Krastev, K., Maltchev, S., Dimitrov, P., Mitrofanov, I., Malahov, A., Golovin, D., Mokrousov, M., Sanin, A., Litvak, M., Kozyrev, A., Tretyakov, V., Nikiforov, S., Vostrukhin, A., Fedosov, F., Grebennikova, N., Zelenyi, L., Shurshakov, V., and Drobishev, S. (2018). Charged particles radiation measurements with Liulin-MO dosimeter of FREND instrument aboard ExoMars Trace Gas Orbiter during the transit and in high elliptic Mars orbit. *Icarus*, 303:53–66.

Shibata, K. and Magara, T. (2011). Solar Flares: Magnetohydrodynamic Processes. *Living Reviews in Solar Physics*, 8(1):6.

Svestka, Z. (1986). On the varieties of solar flares. In Neidig, D. F. and Machado, M. E., editors, *The Lower Atmosphere of Solar Flares*, pages 332–355.

Temmer, M. (2021). Space weather: the solar perspective: An update to Schwenn (2006). *Living Reviews in Solar Physics*, 18(1):4.

Thalmann, J. K., Moraitis, K., Linan, L., Pariat, E., Valori, G., and Dalmasse, K. (2019). Magnetic Helicity Budget of Solar Active Regions Prolific of Eruptive and Confined Flares. *ApJ*, 887(1):64.

Warmuth, A. and Mann, G. (2004). The Application of Radio Diagnostics to the Study of the Solar Drivers of Space Weather. In Scherer, K., Fichter, H., and Heber, B., editors, *Lecture Notes in Physics, Berlin Springer Verlag*, volume 656, page 49.

Webb, D. F. and Howard, T. A. (2012). Coronal Mass Ejections: Observations. *Living Reviews in Solar Physics*, 9:3.

Wild, J. P., Smerd, S. F., and Weiss, A. A. (1963). Solar Bursts. *ARA&A*, 1:291.